The crystal chemistry of the solid solution series between chalcostibite ($CuSbS_2$) and emplectite ($CuBiS_2$)

M. F. RAZMARA, C. M. B. HENDERSON, R. A. D. PATTRICK

Department of Earth Sciences, University of Manchester, Manchester, M13 9PL, UK

A. M. T. BELL* AND J. M. CHARNOCK

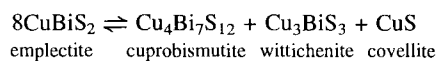Daresbury Laboratory, Warrington, WA4 4AD, UK

Abstract

Sulphosalts in the system $CuSbS_2$–$CuBiS_2$ (chalcostibite–emplectite) form a complete solid solution series. Seven compositions with the general formula $Cu(Sb_xBi_{1-x})S_2$ have been synthesized using dry methods at 310°C. All members of the series are orthorhombic (space group $Pnma$) and show smoothly increasing a and b cell parameters with substitution of Bi for Sb; the c cell parameter increases up to 50% $CuBiS_2$ substitution and then becomes constant. DSC experiments on $CuBiS_2$ show an endothermic heat effect (2.45 kJ/mol.) at 472°C due to the breakdown reaction to Cu_3BiS_3 (wittichenite) plus Bi_2S_3 (bismuthinite). With the addition of 10% $CuSbS_2$ to $CuBiS_2$, the decomposition temperature increases and the endothermic peak is broadened but the energy remains essentially the same (2.53 kJ/mol.). No evidence of this decomposition was observed when the amount of the $CuSbS_2$ component was >30%. The local structure and co-ordination of Cu in the samples were studied by EXAFS analysis of the Cu-K edge but no significant variation occurs in the local Cu environment. The Debye-Waller factor for the first shell of S atoms surrounding Cu in end member $CuSbS_2$ tends to be slightly smaller than for the intermediate solid solutions, suggesting that the tetrahedral Cu environments in the intermediate composition samples is somewhat more disordered than in the end-member. The low expansion characteristics along c appear to be controlled by the linkages between the (CuS_3 + BiS_2) sheets perpendicular to c being relatively inflexible.

KEYWORDS: chalcostibite, emplectite, crystal chemistry, sulphosalts.

Introduction

THE binary systems Cu_2S–Sb_2S_3 and Cu_2S–Bi_2S_3 have been the subject of comprehensive studies but the only investigation of the solid solution series $CuSbS_2$ (chalcostibite)–$CuBiS_2$ (emplectite) is that of Chen and Chang (1971). They reported that in the system Cu_2S–Sb_2S_3–Bi_2S_3, $CuSbS_2$ and $CuBiS_2$ do not form a complete solid solution series, rather an immiscibility gap was reported at the Bi-rich end. Further investigations have been inhibited because

* Current address: Department of Chemistry, Lensfield Road, Cambridge CB2 1EP

the synthesis of emplectite from pure elements, or from Cu_2S + Bi_2S_3, is very sluggish, particularly if the high temperature form, cuprobismutite, is involved in the re-equilibration process (Wang, 1989). Another major problem is the transformation of emplectite to cuprobismutite ($Cu_4Bi_7S_{12}$) at 317°C by the reaction which can be written as:

$$8CuBiS_2 \rightleftharpoons Cu_4Bi_7S_{12} + Cu_3BiS_3 + CuS$$
emplectite cuprobismutite wittichenite covellite

Emplectite is orthorhombic $Pnma$ with a = 6.1426(3), b = 3.9189(4) and c = 14.5282(7) Å (Portheine and Nowacki, 1975). Chalcostibite is the Sb-analogue of emplectite and has the same $Pnma$ space group with a = 6.0211(13), b = 3.7992(6) and c

= 14.509(3) Å (Lind and Makovicky, 1982). The crystal structures are identical with Bi (or Sb) forming trigonal pyramids linked to three S atoms at similar distances (2.5—2.6 Å), and with two more S atoms at greater distances (3.1—3.2 Å) forming distorted square pyramids (Grigas *et al.*, 1975). These pyramids are linked to form chains of BiS_2 parallel to *b*. The $Cu-S_4$ tetrahedra are corner linked, also forming chains of CuS_3 parallel to *b*. These two types of chains are linked to form sheets perpendicular to *c*. An (010) projection of the structure is shown in Fig. 1.

In this paper we report the synthesis of a new solid solution series between emplectite and chalcostibite. The structures of the solid solutions are characterized by analogy with the end-member phases.

Experimental methods

Synthesis

The investigated compounds $Cu(Sb_xBi_{1-x})S_2$, in which *x* was varied from 0 to 1 in increments of 0.1, were obtained using the standard technique of dry sulphide synthesis in which samples are sealed under vacuum in quartz glass tubes. Syntheses were carried out by solid-state reaction of mixtures of high purity (99.99%) Cu, Sb, Bi and S powders, having the stoichiometric compositions of the desired end products. Two synthesis methods were used. In the first, the charges were heated at 310°C in a horizontal furnace for 8 days, and quenched rapidly in liquid nitrogen. To expedite complete reaction, tubes were opened and the samples finely ground under acetone. These powders were sealed in new tubes, reheated for 20 days at the same temperature and then quenched in liquid nitrogen. In the second method, the charges were first raised above the melting temperature, after which the temperature was decreased to 310°C and held for 5 days before the samples were quenched in liquid nitrogen. Emplectite and $Cu(Sb_{0.1}Bi_{0.9})S_2$ could only be synthesized by method one, while chalcostibite and all the other intermediate solid solutions could be made by both methods.

The resulting products were examined by means of powder X-ray diffraction (XRD), electron probe microanalysis (EPMA), differential scanning calorimetry (DSC), and X-ray absorption spectroscopy
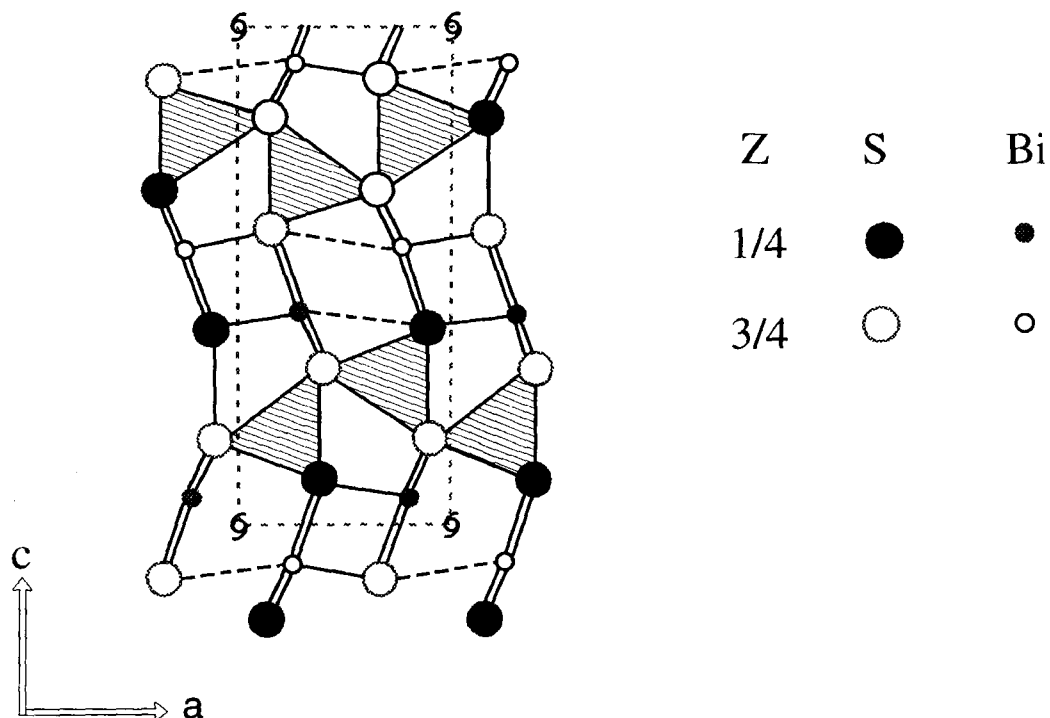

FIG. 1. Structure of emplectite projected perpendicular to *b*. The CuS_4 tetrahedra are shaded. $BiS_2 + CuS_3$ units are linked to form sheets perpendicular to *c*. (After Portheine and Nowacki, 1975).

(XAS), specifically extended X-ray absorption fine structure spectroscopy (EXAFS).

Powder X-ray diffraction

Laboratory X-ray powder diffraction techniques were used to check the structural nature of the reaction products and to obtain unit cell parameters. Lattice parameters were measured at room temperature on a Philips PW1730 diffractometer computer controlled system (PAXRD.2000) operated in the vertical θ–2θ configuration using Cu-$K\alpha$ radiation (1.5418 Å) generated at 40 kV and 20 mA. The samples were smeared on glass slides using amyl acetate, then dried in air. All samples were run with an internal standard of Si (a = 5.43088 Å). The step increment for all synthetic compounds was $0.1°2\theta$ for counting times of 1 second. The refinements were carried out in space group $Pnma$ (JCPDS cards: emplectite 43-1473; chalcostibite 24-347), using the least-squares program CELL4.

High-resolution, synchrotron X-ray powder diffraction was used to determine the structures for the end-members using station 2.3 at the Daresbury laboratory (Cernik $et\ al.$, 1990; Collins $et\ al.$, 1992). The samples were loaded onto an aluminium flat plate container 15 mm in diameter and 1 mm deep. Data were collected at room temperature over the range of 10–$80°2\theta$, $0.01°$ step, 2 s per point, using radiation of wavelength 1.45051 Å. The structure was refined by the Rietveld method (Rietveld, 1969) using MPROF in the Powder Diffraction Program Library (Murray $et\ al.$, 1990). The background was subtracted by interpolation between measured background points with the remaining background being fitted by a 2-term polynomial function; peak profiles were fitted using a pseudo-Voigt function. R-factors for the refined structures are given in Table 2; the presence of impurity phases accounts for these being relatively high.

EPMA

The synthetic compounds were analysed using a Cameca Camebax electron probe controlled by a Link Systems AN10,000 computer and analysing system using an accelerating voltage of 20 kV, beam current 15 nA, beam diameter 3–4 μm, and wavelength dispersive spectrometry. Data reduction was carried out using the ZAF procedure. Mineral standards (and lines used) for Sb-$L\alpha_1$, Bi-$M\alpha_1$, Cu-$K\alpha_1$ and S-$K\alpha_1$, were synthetic chalcostibite ($CuSbS_2$), metallic Cu, synthetic matildite (α-$AgBiS2$) and sphalerite (ZnS). The resulting data are averages of nine to ten spots from each crystal; most of the crystals appeared to be chemically homogeneous.

Thermal analysis

Phase transitions in the $Cu(Sb_xBi_{1-x})S_2$ phases were studied using a PL Thermal Sciences DSC 1500 which consists of TG and DSC modular units. Experiments were carried out at a fixed heating rate of 10°C/min and argon flow of 30 ml/min. Powdered samples were run at temperatures between 20 and 550°C. Runs were performed using ceramic pans and lids (instead of platinum) to make sure there is no reaction between the container and sulphides. Sample masses were in the range 10–20 mg. Each weighed sample was heated only once. X-ray diffraction of samples was undertaken before and after each DSC run. Instrument baseline measurements were obtained from experiments carried out using an empty ceramic pan and subtracted from the sample spectra to obtain reproducible DSC data.

EXAFS

Extended X-ray absorption fine structure (EXAFS) spectroscopy experiments were performed at the Daresbury Synchrotron Radiation Source (SRS), operating in multibunch mode at an energy of 2 GeV with an average current of 150 mA. Samples were finely ground under acetone, diluted with boron nitride, and mounted in aluminium sample cells with Sellotape windows. Cu K-edge EXAFS spectra were collected at room temperature in transmission mode on station 7.1 using a Si (111) double crystal monochromator detuned to 50% rejection of the incident beam in order to remove harmonic contamination. A Bi L_3-edge spectrum of end-member $CuBiS_2$ was collected in transmission mode on station 9.2, using a Si (220) monochromator detuned to 50% rejection.

The raw data were summed in the Daresbury program EXCALIB and background subtracted using EXBACK. The isolated k^3-weighted EXAFS data were analysed using EXCURV92 (Binsted $et\ al.$, 1991), employing the single scattering spherical wave theory (Lee and Pendry, 1975; Gurman $et\ al.$, 1984). Phaseshifts were derived from $ab\ initio$ calculations using Hedin-Lundqvist potentials and von Bart ground states (Hedin and Lundqvist, 1969). For each spectrum a theoretical fit was obtained by adding shells of backscattering atoms around the central absorber atom and iterating the absorber-scatterer distances, R, the Fermi energy correction, E_f, and the Debye-Waller type factors, $2\sigma^2$, to get the best agreement with the experimental data. The Debye-Waller factors include contributions from the thermal motion of the absorber-scatterer pairs and also a static contribution from any variation in R between the scatterers in one shell. The number of atoms in each shell of backscatterers was fixed at the known crystallographic value.

M. F. RAZMARA *ET AL.*

Table 1. EPMA analyses of $CuSbS_2$ –$CuBiS_2$ solid solutions

| Exp. No. | Weight percent | | | | Total | Theoretical formula* | Experimental formula[†] |
	Cu	Sb	Bi	S			
C31	25.57	48.27	—	25.05	99.05	$CuSbS_2$	$Cu_{1.03}Sb_{1.02}S_2$
BS9	23.81	39.42	12.09	22.80	98.05	$Cu(Sb_{0.9}Bi_{0.1})S_2$	$Cu_{1.00}(Sb_{0.90}Bi_{0.16})S_2$
BS7	22.96	35.19	22.32	22.43	101.07	$Cu(SB_{0.7}Bi_{0.3})S_2$	$Cu_{1.03}(Sb_{0.78}Bi_{0.28})S_2$
BS6	22.11	23.01	32.60	21.20	99.27	$Cu(Sb_{0.6}Bi_{0.4})S_2$	$Cu_{1.00}(Sb_{0.57}Bi_{0.47})S_2$
BS5	22.12	21.80	35.13	21.33	100.45	$Cu(Sb_{0.5}Bi_{0.5})S_2$	$Cu_{1.02}(Sb_{0.50}Bi_{0.50})S_2$
BS4	20.49	17.70	41.94	20.91	101.08	$Cu(Sb_{0.4}Bi_{0.6})S_2$	$Cu_{1.01}(Sb_{0.45}Bi_{0.62})S_2$
BS3	20.00	12.00	48.16	19.41	99.62	$Cu(Sb_{0.3}Bi_{0.7})S_2$	$Cu_{1.04}(Sb_{0.33}Bi_{0.76})S_2$
BS1	17.87	5.63	55.27	18.41	97.18	$Cu(Sb_{0.1}Bi_{0.9})S_2$	$Cu_{0.98}(Sb_{0.16}Bi_{0.92})S_2$

* Nominal composition.
[†] Analysed stoichiometry based on 2 S atoms.

Results and discussion

The EPMA analyses showed that solid solution phases are homogeneous with compositions close to their theoretical values (Table 1). Some impurity phases were found; skinnerite (Cu_3SbS_3) in the most Sb-rich samples and wittichenite (Cu_3BiS_3) in the most Bi-rich samples. Note that the amounts of impurities were lower than could be identified by XRD (< about 5%).

The DSC experiments showed a composition effect related to changing Sb content. In pure emplectite, the first strong endothermic reaction detected was initiated at about 472°C and has an energy of 2.45 kJ/mol. (Fig. 2). One sample was heated in the DSC to just above the 472°C heat effect and then cooled. X-ray study showed the presence of wittichenite plus bismuthinite consistent with the decomposition reaction:

Table 2. Fractional atomic coordinates X, Y, Z and isotropic thermal parameters (B) for emplectite and chalcostibite

a: Emplectite. Data from: 1 – This study; 2 – Hofmann (1933)

| | X | | Y | | Z | | B, $\mathring{A}^2$ | |
	1	2	1	2	1	2	1	2
Cu	0.746(2)	0.7509(4)	0.75	0.75	0.1721(5)	0.1719(2)	0.9(2)	2.29
Bi	0.2318(4)	0.23156(1)	0.25	0.25	0.0638(2)	0.06304(4)	0.5	1.64
S_1	0.647(2)	0.6362(6)	0.25	0.25	0.102(1)	0.0980(2)	1.0	1.61
S_2	0.129(2)	0.1258(6)	0.75	0.75	0.182(1)	0.1777(2)	1.0	1.66

b: Chalcostibite: 1 – This study; 2 – Portheine and Nowacki (1975)

| | X | | Y | | Z | | B, $\mathring{A}^2$ | |
	1	2	1	2	1	2	1	2
Cu	0.7463(6)	0.750	0.75	0.75	0.1721(2)	0.17500	2.20(9)	—
Sb	0.2245(2)	0.238	0.25	0.25	0.0636(1)	0.06250	0.5	—
S_1	0.624(1)	0.625	0.25	0.25	0.0960(4)	0.09700	1.0	—
S_2	0.131(1)	0.125	0.75	0.75	0.1787(5)	0.17500	1.0	—

This work: $CuBiS_2$ R_I = 14.9; R_{WP} = 20.2; R_{EXP} = 8.0
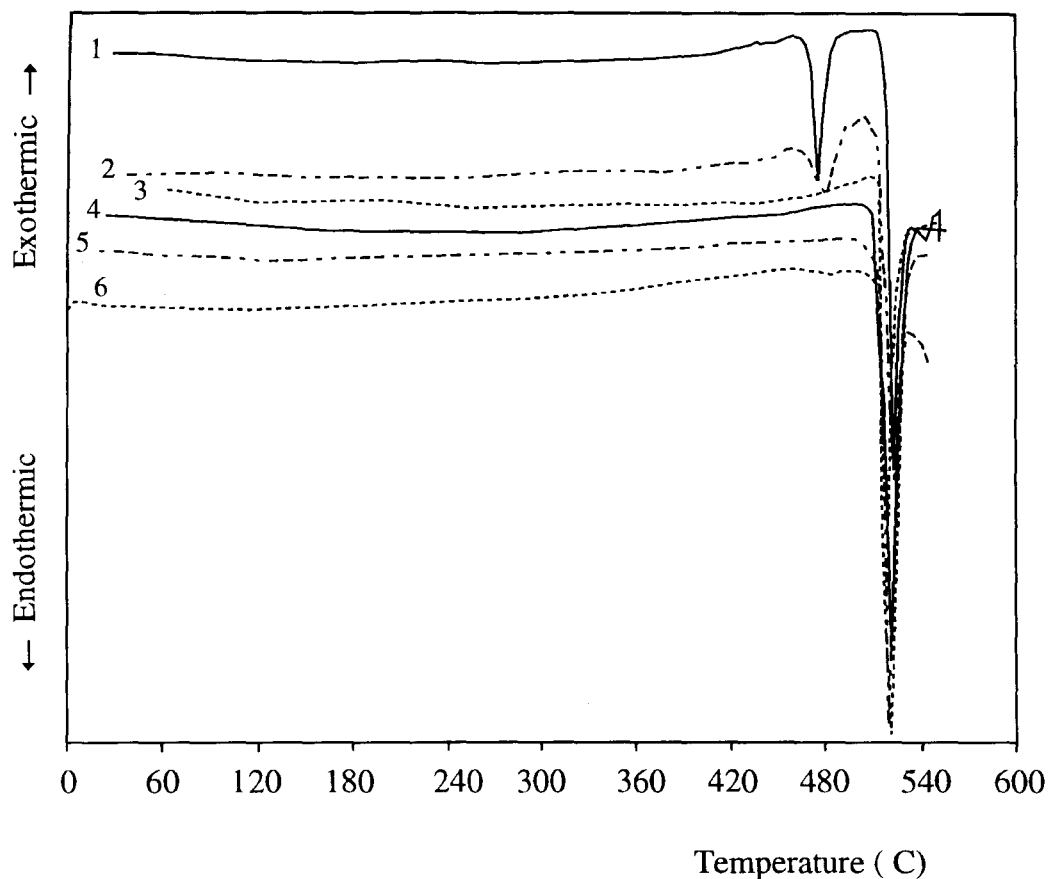$CuSbS_2$ R_I = 26.8; R_{WP} = 23.5; R_{EXP} = 11.5

FIG. 2. DSC curves for emplectite and members of the solid solution series: (1) $CuBiS_2$; (2) $Cu(Bi_{0.9}Sb_{0.1})S_2$; (3) $Cu(Bi_{0.7}Sb_{0.3})S_2$; (4) $Cu(Bi_{0.5}Sb_{0.5})S_2$; (5) $Cu(Bi_{0.3}Sb_{0.7})S_2$; (6) $Cu(Bi_{0.1}Sb_{0.9})S_2$. The endothermic heat effects at about 470°C are due to samples breaking down to wittichenite and bismuthinite, while those at about 520°C are due to melting.

$$3CuBiS_2 \rightleftharpoons Cu_3BiS_3 + Bi_2S_3$$
emplectite   wittichenite   bismuthinite

Within the solid solution series, 10% of the $CuSbS_2$ component markedly broadens the heat effect peak, although the associated energy (2.53 kJ/mol.) is essentially the same as that for emplectite, and increases the decomposition temperature by about 10°C. With 30% of the Sb component, no decomposition was detected (Fig. 2). Note that at the heating rate used (10°C/min), no heat effect was detected at the transformation temperature of emplectite to cuprobismutite (317°C); apparently the kinetics of the nucleation and growth are too sluggish for the latter reaction to proceed on the time scale of the DSC experiments. The endothermic peaks at about 520°C show that all samples melt at essentially the same temperature.

The atomic coordinates determined by synchrotron X-ray powder diffraction for the end members are given in Table 2 where they can be compared with literature data. Bond lengths and bond angles for the present samples and published data are summarized in Table 3. The agreement between observed and calculated profiles for our structural data for $CuBiS_2$ is shown in Fig. 3. The mean Cu–S bond lengths in the two end members are identical, within error, and the limited ranges in intratetrahedral angles show that the CuS_4 tetrahedra in both samples are only slightly distorted.

The cell parameters obtained at room temperature are given in Table 4. The a and b cell parameters and

TABLE 3. Structure parameters for end-member chalcostibite and emplectite

	Chalcostibite (This study)	Chalcostibite (Hofmann, 1933)	Emplectite (This study)	Emplectite (Portheine and Nowacki, 1975)
Cu-S(1) × 2	2.317(4)	2.326	2.291(9)	2.343(3)
Cu-S(2)	2.318(7)	2.254	2.36(2)	2.304(5)
Cu-S(2)′	2.272(8)	2.295	2.24(2)	2.317(5)
Average	2.306	2.275	2.300	2.327
Cu-Bi	−	−	3.429(8)	3.415(3)
Cu-Sb	3.422(3)	−	−	−
Bi-S(1)	−	−	2.61(1)	2.536(4)
Bi-S(2) × 2	−	−	2.68(1)	2.653(2)
Bi-S(1) × 2	−	−	3.19(1)	3.158(8)
Sb-S(1)	2.451(6)	2.436	−	−
Sb-S(2) × 2	2.590(5)	2.656	−	−
Sb-S(1) × 2	3.129(5)	−	−	−
S(1)-Cu-S(1)	110.1(2)	−	117.6(6)	113.50(16)
S(1)-Cu-S(2) × 2	109.7(1)	−	107.0(4)	109.43(12)
S(1)-Cu-S(2)′ × 2	110.9(2)	−	109.6(4)	109.43(12)
S(2)-Cu-S(2)	105.4(3)	−	105.2(6)	107.28(17)
Cu-S(1)-Cu	110.1(3)	−	117.6(6)	113.50(17)
Cu-S(2)-Cu	110.2(5)	−	112.2(7)	111.47(18)

cell volume show smooth increases with increasing Bi content, but the *c* dimension reaches a maximum value at $Cu(Bi_{0.5}Sb_{0.5})S_2$ (Fig. 4). This trend of cell parameters is to be expected as Bi is larger than Sb (ionic radii 0.96 Å and 0.80 Å for Bi and Sb, respectively). However, note that the expansion is highly anisotropic with that along *c* (perpendicular to the stacking of the sheets), being only 20% of those in the *a* and *b* directions up to the $Cu(Bi_{0.5}Sb_{0.5})S_2$ composition, after which *c* shows no further change.

The EXAFS provides element specific, averaged short range structural information on the radial environment surrounding the target element on a

length scale up to about 8 Å, depending on the material being studied. Thus it is possible to obtain bond lengths to surrounding shells of atoms, as well as co-ordination numbers and disorder parameters (Debye-Waller factors). In contrast to EXAFS which is usually a single scattering phenomenon, the near edge structure (XANES) results from multiple scattering, and therefore gives longer range structural information. See Brown *et al.* (1988) for further details of X-ray absorption spectroscopy.

Refined Bi L_3-edge EXAFS data for end member emplectite are summarized in Table 5 together with radial crystal structure data around Bi calculated

TABLE 4. Cell parameters for the $CuSbS_2$–$CuBiS_2$ solid solution series

Sample Number	Composition	Cell parameters			Cell volume (Å³)
		a (Å)	*b* (Å)	*c* (Å)	
C31	$CuSbS_2$	6.0160(1)*	3.7968(6)	14.499(3)	331.176(7)
BS9	$Cu(Sb_{0.9}Bi_{0.1})S_2$	6.0287(2)	3.8081(1)	14.500(4)	332.89(1)
BS7	$Cu(Sb_{0.7}Bi_{0.3})S_2$	6.0454(1)	3.8276(6)	14.519(2)	335.963(7)
BS5	$Cu(Sb_{0.5}Bi_{0.5})S_2$	6.0661(1)	3.8520(6)	14.526(2)	339.417(7)
BS3	$Cu(Sb_{0.3}Bi_{0.7})S_2$	6.0954(3)	3.8726(2)	14.525(5)	342.867(2)
BS1	$Cu(Sb_{0.1}Bi_{0.9})S_2$	6.1228(2)	3.8931(2)	14.523(1)	346.176(1)
E31	$CuBiS_2$	6.1413(5)	3.9191(5)	14.524(2)	349.588(5)

* Numbers in parentheses are 1 sigma standard deviations.
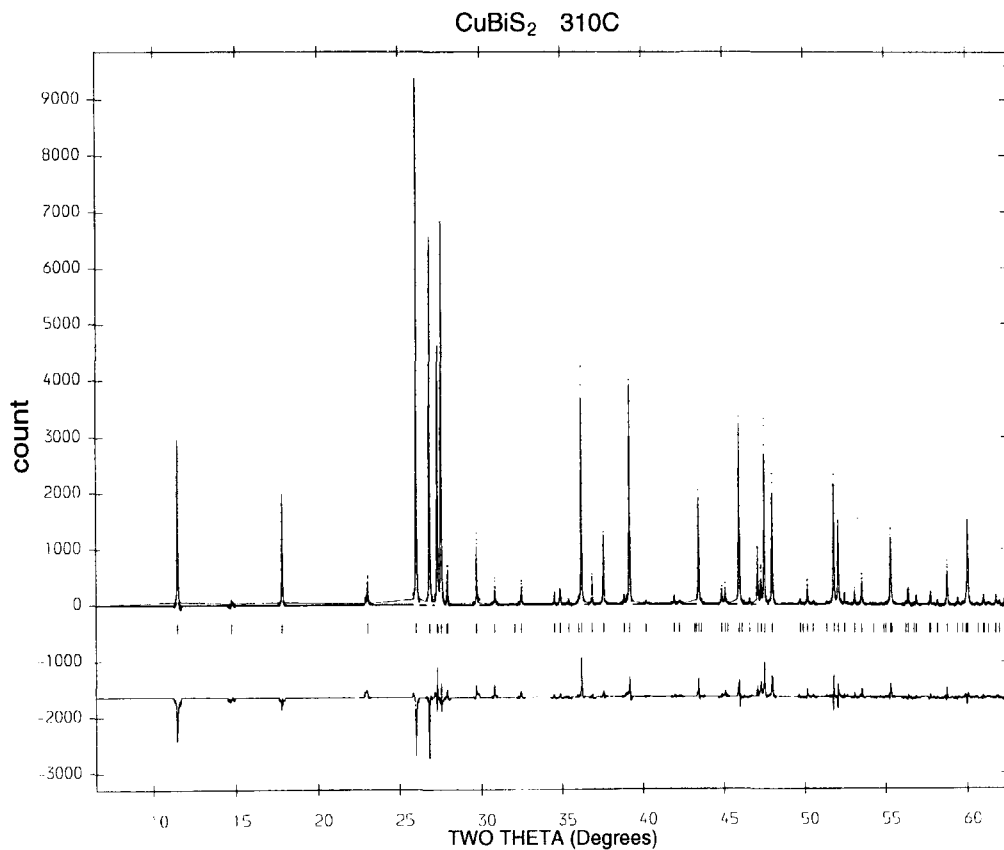
CuBiS₂ 310C

FIG. 3. Comparison of experimental (dots) and calculated (solid line) diffraction patterns for CuBiS₂, together with the difference plot (below) and theoretical peak positions (above).

from the data of Portheine and Nowacki (1975). The Bi EXAFS data show the presence of several shells due to scattering from the three S atoms forming the trigonal pyramid with Bi, the two further S atoms belonging to the square pyramid polyhedron, and the closest Cu atom (Fig. 5). Mean EXAFS Bi-S bond lengths show satisfactory agreement with crystallographic data.

The Cu-XANES spectra are closely similar throughout the solid solution series showing that the multiple scattering from the outer shells around Cu is not affected by changing Bi-Sb contents (Fig. 6). The

TABLE 5. Comparison of crystal structure of emplectite, CuBiS₂, with EXAFS parameters for the Bi L_3-edge spectrum

| Shell | Crystal structure | | EXAFS | |
	R (Å)	R range (Å)	R (Å)*	D.W. (Å²)#
3 × S	2.614	2.536–2.653	2.59	0.019
2 × S	3.158	–	3.11	0.029
1 × Cu	3.415	–	3.48	0.024

* R = Average bismuth – scatterer bond length ± 0.02 Å first shell, ± 0.05 Å outer shells
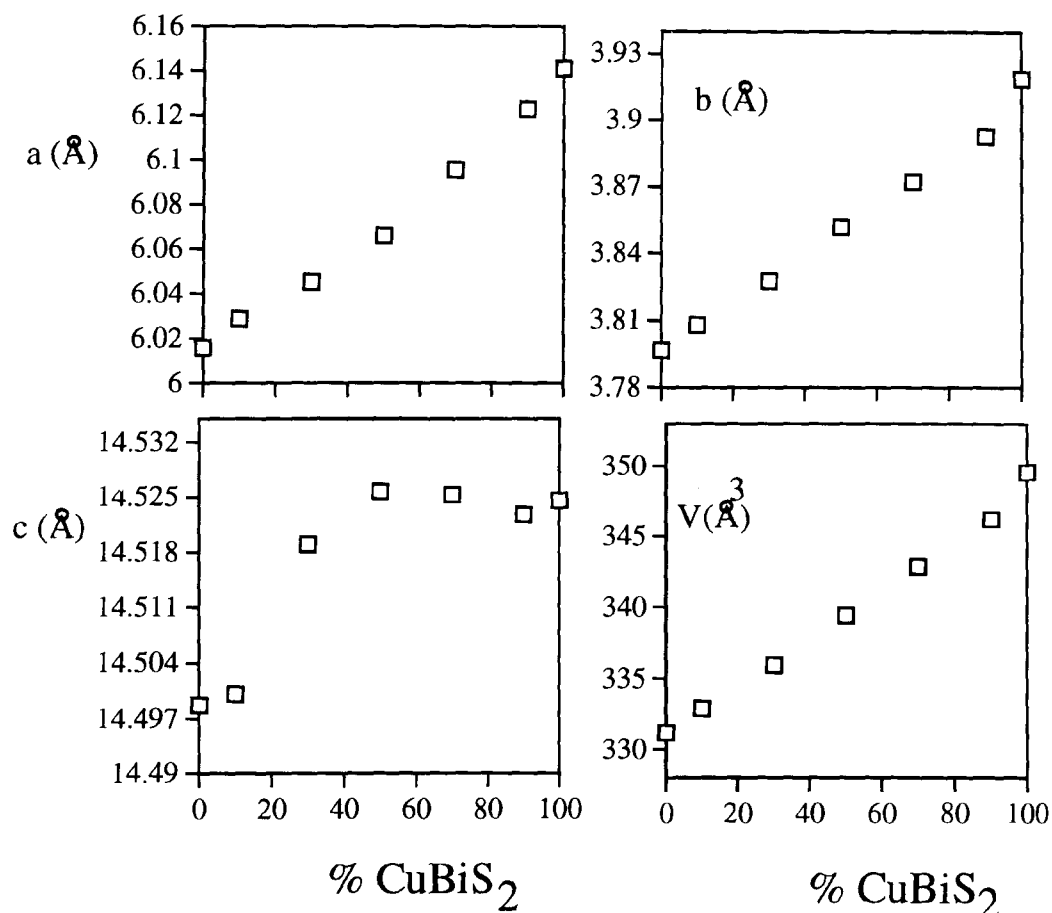\# D.W. = Debye-Waller factor, $2\sigma^2$ ($\pm$ 0.004 Å²)

M. F. RAZMARA *ET AL.*

Fig. 4. Cell parameter variations with composition in the solid solution series $CuSbS_2$–$CuBiS_2$. Note that the c parameter becomes constant when approximately half of the Sb has been substituted by Bi.

EXAFS spectra for end-member $CuSbS_2$ and the solid solutions are closely similar and appear to consist of single sine waves, suggesting that only one shell of scatterers around Cu can be detected (Fig. 7a). This is confirmed in the Fourier transforms (Fig. 7b) by the presence of single peaks. This shell consists of the nearest neighbour S atoms. In addition, no significant difference in the overall structure around Cu between $CuSbS_2$ and the solid solutions is apparent, consistent with Cu being 4 co-ordinated in all samples. Refined first shell Cu-S bond lengths and Debye-Waller factors, for a fixed co-ordination number of 4, are given in Table 6. The mean Cu-S in end-member $CuSbS_2$ is equal to 2.29 Å, within error of the value obtained by XRD. Assuming a relative error in the Cu-S bond length of 0.01 Å, it seems that in the solid solutions the mean Cu-S bond lengths show no significant variations. Although the variation in

Debye-Waller factors is small (Table 6), it is possible that the slightly higher values for the solid solutions indicate that the Cu tetrahedral environment in these samples is somewhat more distorted than that in the $CuSbS_2$ end-member.

The fact that the Cu-S bond lengths do not vary throughout the solid solution series suggests that unit cell expansion on substituting Bi for Sb is entirely due to the mean Bi-S bond being about 6% longer than Sb-S. However, the much reduced expansion along c compared with those along the a and b axes, together with the c axis achieving a maximum value with 50% substitution of Bi for Sb (Fig. 4), suggests that the Sb,Bi-S polyhedra become increasingly distorted in the solid solution series. Thus the 'short' Sb,Bi-S bond lengths parallel to c (Fig. 1) apparently show very little variation whereas the longer Sb,Bi-S bonds along a and b expand as
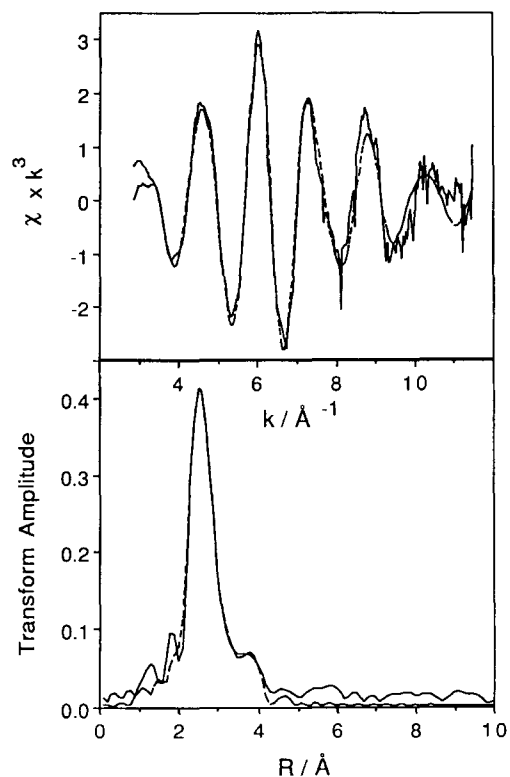
FIG. 5. Refined Bi $L3$-edge data for $CuBiS_2$: k^3 XAFS spectrum above and Fourier Transform below. Experimental data — solid lines; best-fits — broken lines.

TABLE 6. Refined Cu K-edge structural parameters for the $CuSbS_2$–$CuBiS_2$ solid solution series

	Composition	$R(\text{Å})^*$	$N^\$$	$D.W.(\text{Å}^2)^\#$
C31	$CuSbS_2$	2.29	4.0	0.014
BS9	$Cu(Sb_{0.9}Bi_{0.1})S_2$	2.27	4.0	0.018
BS7	$Cu(Sb_{0.7}Bi_{0.3})S_2$	2.29	4.0	0.015
BS5	$Cu(Sb_{0.5}Bi_{0.5})S_2$	2.29	4.0	0.013
BS3	$Cu(Sb_{0.3}Bi_{0.7})S_2$	2.29	4.0	0.016
BS1	$Cu(Sb_{0.1}Bi_{0.9})S_2$	2.29	4.0	0.017

* R = Average Cu-S bond lengths for the first coordination shell (relative error $\pm$ 0.001 Å, absolute error $\pm$ 0.002 Å)
$^\$$ N = Fixed coordination number
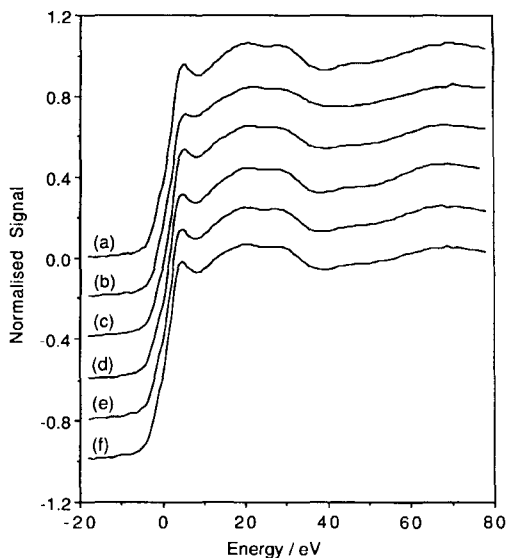$^\#$ D.W. = Debye-Waller factor $2\sigma^2(\pm$ 0.004 Å$^2)$

FIG. 6. Cu K-edge XANES spectra for the solid solution series $CuSbS_2$–$CuBiS_2$: (a) $CuSbS_2$; (b) $Cu(Sb_{0.9}Bi_{0.1})S_2$; (c) $Cu(Sb_{0.7}Bi_{0.3})S_2$; (d) $Cu(Sb_{0.5}Bi_{0.5})S_2$; (e) $Cu(Sb_{0.3}Bi_{0.7})S_2$; (f) $Cu(Sb_{0.1}Bi_{0.9})S_2$.

expected because of the differences in atomic sizes of Sb and Bi. It seems that the linking of the 'sheets' perpendicular to c is a relatively inflexible aspect of the crystal structure.

Conclusions

Despite earlier reports, a complete solid solution series can be synthesized between $CuSbS_2$ and $CuBiS_2$. The unit cell expands anisotropically, with the c dimension showing limited variation, reaching a maximum value when about half of the Sb is substituted by Bi. The Cu-S tetrahedral environment shows no significant variation across the solid solution, suggesting that the low expansion characteristics along c are controlled by the linkages between the CuS_3 + BiS_2 sheets perpendicular to c being relatively inflexible.

Acknowledgement

References

Binsted, N., Campbell, J.W., Gurman, S.J. and Stephenson, P.C. (1991) CCLRC Daresbury Laboratory EXCURV program.
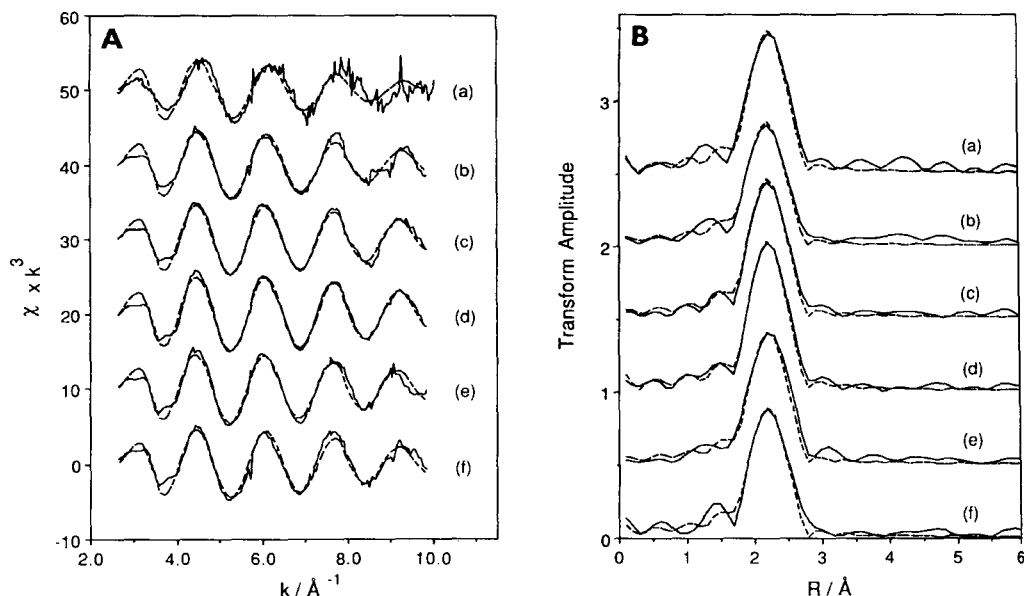
FIG. 7. Refined Cu K-edge XAS spectra for the solid solution series $CuSbS_2$–$CuBiS_2$: (A) k^3 XAFS; (B) Fourier Transforms. Spectra labelling: (a) $CuSbS_2$; (b) $Cu(Sb_{0.9}Bi_{0.1})S_2$; (c) $Cu(Sb_{0.7}Bi_{0.3})S_2$; (d) $Cu(Sb_{0.5}Bi_{0.5})S_2$; (e) $Cu(Sb_{0.3}Bi_{0.7})S_2$; (f) $Cu(Sb_{0.1}Bi_{0.9})S_2$. Experimental data — solid lines; best-fits — broken lines. Note that the signal:noise: ratio in spectrum (a) is somewhat poorer than in the other spectra.

Brown, G.E., Jr., Calas, G., Waychunas, G.A. and Petiau, J. (1988) X-ray absorption spectroscopy and its application in mineralogy and geochemistry. *Reviews in Mineralogy* (Min. Soc. Amer.), **18**, 431–512.

Chen, T.T. and Chang, L.L.Y. (1971) Phase relations in the systems Ag_2S–Sb_2S_3–Bi_2S_3 and Cu_2S–Sb_2S_3–Bi_2S_3. *Geol. Soc. Amer. Abstr. Program*, **3**(7), 524.

Cernik, R.J., Murray, P.K., Pattison, P. and Fitch, A.N. (1990) A two-circle powder diffractometer for synchrotron radiation with a closed loop encoder feedback system. *J. Appl. Crystallogr.*, **23**, 292–6.

Collins, S.P., Cernik, R.J., Pattison, P., Bell, A.M.T. and Fitch, A.N. (1992) A two-circle powder diffractometer for synchrotron radiation on station 2.3 at the SRS. *Rev. Sci. Instrum.*, **63**, 1013–4.

Grigas, I., Mozgova, N.N., Orlyukas, A. and Samulenis, V. (1975) The phase transition in $CuSbS_2$ crystals. *Sov. Phys. Crystallogr.*, **20**, 741–2.

Gurman, S.J., Binsted, N. and Ross, I. (1984) A rapid, exact, curved wave theory for EXAFS calculations. *J. Phys. C: Solid State Phys.*, **17**, 143–51.

Hedin, L. and Lundqvist, S. (1969) Effects of electron-electron and electron-phonon interactions on the one-electron states of solids. *Solid State Phys.*, **23**, 1–181.

Hofmann, W. (1933) Strukturelle und morphologische zusammenhaenge bei erzen vom formeltyp ABC_2 I. Die struktur von wolfsbergit $CuSbS_2$ and emplektit $CuBiS_2$ und deren Beziehungen zu der struktur von Antimonit Sb_2S_3. *Z. Kristallogr.*, **84**, 177–203.

Lee, P.A. and Pendry, J.B. (1975) Theory of the extended X-ray absorption fine structure. *Physical Review*, **B11**, 2795–811.

Lind, I.L. and Makovicky, E. (1982) Phase relations in the system Cu-Bi-S at 200°C, 10^8 Pa by hydrothermal synthesis — microprobe analysis of tetrahedrites — a warning. *Neues Jahrb. Mineral., Abh.*, **145**, 134–56.

Murray, A.D., Cockcroft, J.K. and Fitch, A.N. (1990) Powder Diffraction Program Library (PDPL). Univ. College, University of London.

Portheine, J.C. and Nowacki, W. (1975) Refinement of the crystal structure of emplectite, $CuBiS_2$. *Z. Kristallogr.*, **141**, 387–402.

Rietveld, H.M. (1969) A profile refinement method for nuclear and magnetic structures. *J. Appl. Crystallogr.*, **2**, 65–71.

Wang, N. (1989) Emplectite: Synthesis, powder data and thermal stability. *Neues Jahrb. Mineral. Mh.*, 521–3.